Biophysical Journal Volume 107 October 2014 1930–1938

Article

Effects of Hydroxylated Carbon Nanotubes on the Aggregation of Aβ_{16-22} Peptides: A Combined Simulation and Experimental Study

Luogang Xie,[1] Dongdong Lin,[1] Yin Luo,[1] Huiyu Li,[2] Xinju Yang,[1] and Guanghong Wei[1,*]
[1]State Key Laboratory of Surface Physics, Key Laboratory for Computational Physical Sciences (Ministry of Education), and Department of Physics, Fudan University, Shanghai, China; and [2]Department of Mathematics and Physics, Shanghai University of Electric Power, Shanghai, China

ABSTRACT The pathogenesis of Alzheimer's disease (AD) is associated with the aggregation of amyloid-β (Aβ) peptides into toxic aggregates with β-sheet character. In a previous computational study, we showed that pristine single-walled carbon nanotubes (SWCNTs) can inhibit the formation of β-sheet-rich oligomers in the central hydrophobic core fragment of Aβ (Aβ_{16-22}). However, the poor solubility of SWCNTs in water hinders their use in biomedical applications and nanomedicine. Here, we investigate the influence of hydroxylated SWCNT, a water-soluble SWCNT derivative, on the aggregation of Aβ_{16-22} peptides using all-atom explicit-water replica exchange molecular dynamics simulations. Our results show that hydroxylated SWCNTs can significantly inhibit β-sheet formation and shift the conformations of Aβ_{16-22} oligomers from ordered β-sheet-rich structures toward disordered coil aggregates. Detailed analyses of the SWCNT-Aβ interaction reveal that the inhibition of β-sheet formation by hydroxylated SWCNTs mainly results from strong electrostatic interactions between the hydroxyl groups of SWCNTs and the positively charged residue K16 of Aβ_{16-22} and hydrophobic and aromatic stacking interactions between SWCNTs and F19 and F20. In addition, our atomic force microscopy and thioflavin T fluorescence experiments confirm the inhibitory effect of both pristine and hydroxylated SWCNTs on Aβ_{16-22} fibrillization, in support of our previous and present replica exchange molecular dynamics simulation results. These results demonstrate that hydroxylated SWCNTs efficiently inhibit the aggregation of Aβ_{16-22}; in addition, they offer molecular insight into the inhibition mechanism, thus providing new clues for the design of therapeutic drugs against amyloidosis.

INTRODUCTION

The pathological self-assembly of proteins/peptides into amyloid fibrillar deposits is associated with many human diseases, including Alzheimer's (AD), Huntington's, and Parkinson's diseases (1), among which AD is the most common neurodegenerative disorder. The predominant components of the amyloid deposits in the brains of AD patients are 40- and 42-residue-long amyloid-β (Aβ) peptides (2). It has been shown that amyloid fibrils display a common cross-β structure characterized by β-strands perpendicular to and interstrand hydrogen bonds parallel to the fibril axis (3). Amyloid-β fibrillization is described by a nucleation-elongation-saturation process characterized by a long lag phase of nucleus formation followed by rapid elongation and saturation of fibrils (4). A large number of experimental studies have reported that polymer nanoparticles (5), carbon nanoparticles (6–8), and gold nanoparticles (9,10) can inhibit or enhance amyloid fibrillization, depending on their surface physicochemical properties and the intrinsic aggregate rate of proteins/peptides (11,12).

The influence of carbon nanoparticles (such as carbon nanotubes, fullerenes, and graphenes) on amyloid fibril formation has received great attention in recent years due to the unique architecture of these particles, their exceptional physical properties, and their capacity to cross biological barriers (13–15). Carbon nanotubes (CNTs) are one-dimensional macromolecules consisting of single or multiple concentric sheets of graphene cylinders. Single-walled CNTs (SWCNTs), with diameters of only 0.4–3.5 nm, can easily enter the cytoplasm and nucleus through the lipid bilayer (16) and thus have many biomedical applications, including cellular delivery of peptides/proteins (17), tissue engineering (18), and design of novel biomaterials (19). In particular, recent experimental studies (7,8) indicate that CNTs can affect the amyloid fibrillization of proteins. For example, using thioflavin T (ThT) fluorescence, Linse et al. (8) reported that multiple-walled CNTs significantly enhance the fibrillization rate of β_2-microglobulin by shortening the lag phase for nucleation. In contrast, Ghule et al. (7) found that multiple-walled CNTs prevented 2,2,2-trifluoroethanol-induced amyloid aggregation of the recombinant human acidic fibroblast growth factor protein by providing interaction surfaces for adsorbing or encapsulating proteins. These two contrasting effects of CNTs on the fibrillization of two different peptides indicate that the influence of CNTs on the aggregation of peptides depends on the intrinsic structural properties of the proteins.

Submitted May 1, 2014, and accepted for publication August 21, 2014.
*Correspondence: ghwei@fudan.edu.cn
Luogang Xie and Dongdong Lin contributed equally to this work.
Editor: Bert de Groot.

0006-3495/14/10/1930/9 $2.00
http://dx.doi.org/10.1016/j.bpj.2014.08.034

On the computational side, our previous molecular dynamics (MD) simulations on the amphiphilic peptide Aβ_{25-35} suggested that SWCNTs could inhibit Aβ_{25-35} fibrillization by inducing the formation of β-barrel structures (20). Subsequently, our replica-exchange MD (REMD) simulations on residues 16–22 of Aβ peptide (Aβ_{16-22}) (21) demonstrated that pristine SWCNTs prevented the formation of β-sheet-rich oligomers and dissociated prefibrillar β-sheets into disordered coil aggregates. Using the docking method and MD simulations, Andujar et al. examined the effect of pristine C_{60} on the structural stability of constructed protofibril-like Aβ_{1-42} pentamers and found that C_{60} preferentially bound to the core part of the protofibril and destabilized the structures of the protofibril (22). Guo et al. (23), in an MD simulation study, investigated the influence of carbon nanoparticles on the aggregation of islet amyloid polypeptide fragment 22–28 and observed an inhibitory effect. Adsorption of the full-length Aβ_{1-42} monomer and its mutants on pristine SWCNT was investigated in MD simulations by Jana et al., who proposed that the central hydrophobic core region initiates complete peptide adsorption (24–26). Recently, two independent research groups used MD simulations to examine the influence of dimensionality of pristine carbon nanomaterials (including SWCNT, C_{60}, and graphene) on the binding and dynamics of amyloid and nonamyloid peptide monomers and proposed that binding affinity and dynamics are curvature-dependent (27,28).

These experimental and computational studies have greatly improved our understanding of the adsorption of peptide monomers to carbon nanoparticle surfaces and the effect of CNTs on peptide aggregation. However, the poor solubility of SWCNTs in water has been a major hindrance to their potential biomedical application. Hydroxylated CNTs, due to their enhanced solubility in water, their biocompatibility, and their reduced cytotoxicity compared to pristine CNTs (29), are becoming a more promising candidate for biomedical applications. To our knowledge, the influence of hydroxylated SWCNTs on the aggregation of amyloid peptide has not been reported. In this study, we investigate the effects of hydroxylated SWCNTs on the aggregation of Aβ_{16-22} fragments, as well as the mechanisms involved. Aβ_{16-22} (with amino acid sequence KLVFFAE), containing the central hydrophobic core of Aβ (LVFFA), is one of the shortest peptides that form amyloid fibrils morphologically similar to full-length Aβ fibrils at neutral pH (30). Therefore, it is a good model system for studying the molecular mechanism of nanoparticle-mediated aggregation of Aβ peptides. In this work, we study the octamerization of the Aβ_{16-22} peptide in the absence and presence of hydroxylated SWCNT by performing extensive all-atom REMD simulations with explicit water. The reason for choosing an octamer is that previous all-atom MD studies indicate that the minimum nucleus size consists of at least eight Aβ_{16-22} peptide chains, based on the stability of preformed β-sheet assemblies (31). In addition to REMD simulations, atomic force microscopy (AFM) and ThT fluorescence experiments are employed to monitor the influence of pristine and hydroxylated SWCNTs on the aggregation processes of Aβ_{16-22} peptides. It is found that both pristine and hydroxylated SWCNTs can greatly retard the aggregation of Aβ_{16-22} peptides, in support of our previous (21) and present REMD simulation results.

MATERIALS AND METHODS

Isolated Aβ octamer and Aβ in complex with hydroxylated SWCNT

The Aβ_{16-22} peptide consists of seven amino acid residues, and its N- and C-termini are blocked by acetyl and amine groups, as in an experiment by Balbach et al. (30). To mimic the experimental neutral pH condition, the side chain of Lys is protonated (Lys^+) and that of Glu is deprotonated (Glu^-). The starting state of the Aβ_{16-22} octamer consists of eight random chains (see Fig. S1 *a* in the Supporting Material), similar to our previous studies (21,32). An SWCNT, with a diameter of 0.407 nm and a length of 4.25 nm, is modified uniformly by 30 hydroxyl groups, leading to a hydroxylated SWCNT consisting of 216 carbon atoms and 30 hydroxyl groups (denoted as $SWCNT_{216}(OH)_{30}$). An SWCNT of this length provides a surface sufficient for adsorption by Aβ_{16-22} peptides. The $SWCNT_{216}(OH)_{30}$ is initially placed in the center of the eight peptide chains (see Fig. S1 *d*). For brevity, we will simplify Aβ_{16-22} to Aβ. The isolated Aβ and Aβ+$SWCNT_{216}(OH)_{30}$ complex (see Fig. S1, *a* and *d*) were respectively placed in a box of SPC water molecules (33), with a minimum distance of 0.9 nm to the water-box wall. The total numbers of atoms for the isolated Aβ and Aβ+$SWCNT_{216}(OH)_{30}$ complex are 19,717 and 38,089, respectively.

REMD simulations and analyses

REMD simulations (34) were performed in the isothermal-isobaric (NPT) ensemble using the GROMACS-3.3.3 software package (35) with the GROMOS96 43a1 force field (36), in accordance with previous computational studies of Aβ_{16-22} peptides (21,32,37,38). There are 40 replicas, at temperatures exponentially spaced between 310 K and 420 K. Oxygen and hydrogen atoms in hydroxyl groups and carbon atoms bonded with hydroxyl groups in SWCNT have partial charges of -0.8, $+0.3$, and $+0.5$ $|e|$, respectively, whereas other carbon atoms in the single-walled carbon nanotubol (SWCNT*ol*) are uncharged, in accordance with previous studies (20,21,39). The simulation time for each replica of isolated Aβ and Aβ+$SWCNT_{216}(OH)_{30}$ complex is 200 ns.

Trajectory analysis was performed using our in-house-developed codes and the tools implemented in GROMACS software. All results reported in this study refer to the REMD sampling collected at 310 K. The data in the first 30 ns REMD trajectory were discarded to remove the bias of the initial states. We analyze the REMD trajectories using several parameters, including secondary structure content (via the DSSP program) (40), free-energy landscape (or potential of mean force), percentage of various sizes of β-sheets, number of hydrogen bonds (H-bonds), connectivity length (CL), configuration type (CT), and probability of residue-residue contacts. Among these, two chains are considered to form a β-sheet if 1), at least two consecutive residues in each chain visit the β-strand state; and 2), they have at least two hydrogen bonds (H-bonds). The percentages of various sizes of β-sheet were also calculated. The size of a β-sheet is the number of strands in an n-stranded β-sheet, e.g., the β-sheet size of a two-stranded β-sheet is 2. As in our previous work (21,41), we used a topological parameter, CL, to characterize the structures of Aβ_{16-22} octamers. CL is defined as the sum over the square root of the β-sheet size and the number of disordered chains in each configuration. For example, an assembly of eight disordered chains

has a CL of $8 \times \sqrt{1} = 8$, whereas a bilayer consisting of two four-stranded β-sheets has a CL of $\sqrt{4} + \sqrt{4} = 4$. Thus, the more disordered the aggregate is, the larger the connectivity length becomes. A detailed description of other parameters is given in the Supporting Material. All representations of the studied systems are drawn using the VMD program (42).

AFM and ThT fluorescence experiments

$A\beta_{16-22}$ peptides purchased from GL Biochem (Shanghai, China) were further purified by high-performance liquid chromatography to reach a purity of >95%. High-purity pristine SWCNTs (purity >95 wt %, OD 1–2 nm, length <5 μm) and hydroxylated SWCNTs (purity >90 wt %, OD 1–2 nm, length 1–3 μm, -OH content 3.96 wt %) were purchased from Chengdu Organic Chemicals (Chengdu, China). The peptide solution was prepared by dissolving $A\beta_{16-22}$ in deionized water (resistivity 18.2 MΩ•cm), yielding a concentration of 0.2 mM.

New methods of mixing $A\beta_{16-22}$ peptides and pristine and hydroxylated SWCNTs were applied without using any dispersants. Powdered lyophilized $A\beta_{16-22}$ and SWCNTs, 4 mg each, were fully mixed, and the mixed components were added to 20 mL deionized water and sonicated in ice-cold water for 1 min. The undispersed SWCNTs were then removed and their weight measured. The remainder of the uniformly dispersed solution was incubated at 37°C in a hygrothermostat, where it could be kept stable for several days. Due to the weighing error of the instrument (accuracy 0.01 mg), the content of SWCNTs in the solution could not be given a precise value (pristine SWCNTs, ~0.05 mg/mL; hydroxylated SWCNTs, ~0.1 mg/mL). Detailed descriptions of AFM imaging and ThT fluorescence measurements are given in the Supporting Material.

RESULTS AND DISCUSSION

We first verify the convergence of the REMD runs of isolated Aβ and Aβ+$SWCNT_{216}(OH)_{30}$ systems, which is crucial to the reliability of the results obtained. As shown in Fig. S1, *b* and *e*, the probability density functions (PDFs) of the end-to-end distance of Aβ peptide within the two time intervals (30–115 ns and 115–200 ns) in these two systems overlap very well. We also check sampling efficiency by following the time evolution of temperature swapping of one representative replica in temperature space (Fig. S1, *c* and *f*). One can see that the replicas sufficiently visit the whole temperature space in both the isolated Aβ and Aβ+$SWCNT_{216}(OH)_{30}$ systems. The secondary structure content of Aβ within the two time intervals in these two systems (Fig. S2) is also quite similar, differing by $\leq$ 5%. Among all possible secondary structures, coil and β-sheet are dominant. The average coil probabilities within the two time intervals are 50.2% and 48.8% for Aβ versus 74.4% and 73.5% for Aβ with SWCNT*ol*, and the β-sheet probabilities are 45.5% and 47.8% without SWCNT*ol* and 17.1% and 18.4% with SWCNT*ol*. These data suggest that our two REMD simulations are reasonably converged.

Hydroxylated SWCNTs significantly reduce the β-sheet content and induce the formation of disordered $A\beta_{16-22}$ octamers

$A\beta_{16-22}$ peptides in the isolated Aβ system can form various β-sheet-rich aggregates and have an average β-sheet probability of 46.6%. When the $SWCNT_{216}(OH)_{30}$ is introduced into the isolated Aβ system, the β-sheet content shows a significant decrease from 46.6% (isolated) to 17.5% (complex) and the coil content increases from 49.5% to 74.0%. To examine the influence of $SWCNT_{216}(OH)_{30}$ on the secondary structure of each amino acid residue, we calculated the β-sheet percentage of each residue (see Fig. 1 *a*). Without $SWCNT_{216}(OH)_{30}$, residues L17-V18-F19-F20-A21 have a 40.4~81.9% probability of adopting β-sheet conformation, with V18 and F19 having a high β-sheet probability of 81.8% and 79.7%, respectively. However, with the addition of $SWCNT_{216}(OH)_{30}$, these residues have distinctly reduced β-sheet probabilities of 13.1~32.1%, with probabilities of 29.8% for V18 and 32.1% for F19. These results demonstrate that $SWCNT_{216}(OH)_{30}$ can substantially prevent β-sheet formation of $A\beta_{16-22}$ peptides.

It is noted that the peptide concentration in the isolated Aβ system is 64.74 mM, whereas it is 33.97 mM in the Aβ+$SWCNT_{216}(OH)_{30}$ complex, lower than that of the isolated Aβ system. The choice of an Aβ system with a higher peptide concentration is mainly motivated by a recent computational study by the de Groot group on the oligomerization of the VEALYL peptide from insulin at four different concentrations (3.3, 8.3, 16.6, and 83 mM)) showing that the final structures approached ordered aggregates with steric-zipper-like structural features, irrespective

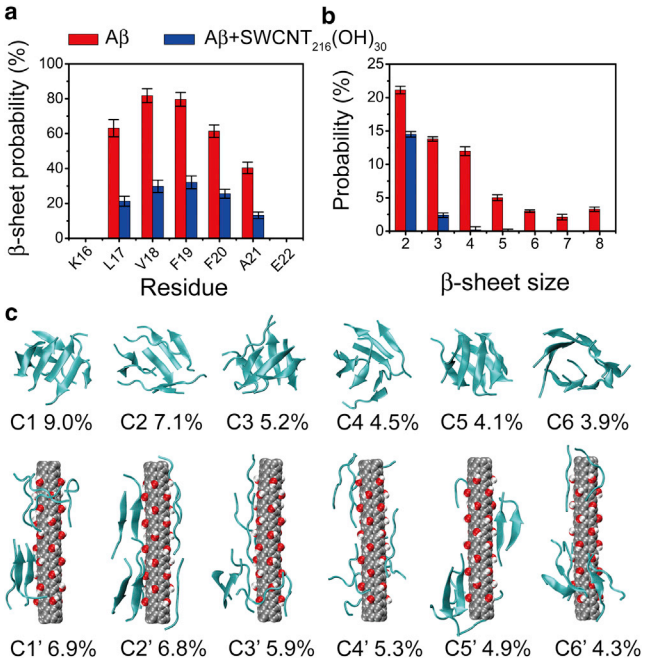

FIGURE 1 Secondary and tertiary structures of $A\beta_{16-22}$ octamer in the absence and presence of $SWCNT_{216}(OH)_{30}$. (*a* and *b*) Calculated β-sheet probability of each residue (*a*) and probability of different β-sheet sizes (*b*) for $A\beta_{16-22}$ octamer in isolated Aβ (*red*) and Aβ+$SWCNT_{216}(OH)_{30}$ (*blue*) systems. (*c*) Representative structures and populations (%) of the first six most populated clusters for $A\beta_{16-22}$ octamer in the absence (*upper*) and presence (*lower*) of $SWCNT_{216}(OH)_{30}$. To see this figure in color, go online.

of the initial peptide concentration (43). Moreover, the choice of $A\beta_{16-22}$ system with the higher peptide concentration enables us to characterize the relatively complete conformational ensembles from simulations using current computer facilities. To examine whether the concentration of $A\beta_{16-22}$ peptides influences β-sheet formation, we performed a 115-ns REMD simulation for the isolated Aβ system with a concentration of 33.80 mM, a concentration very close to that of the Aβ+$SWCNT_{216}(OH)_{30}$ system (33.97 mM). The average β-sheet probability is calculated as 47.3% based on the trajectory data within the last 30–115-ns time interval, extremely close to the β-sheet content of 46.6% for the $A\beta_{16-22}$ system with a concentration of 64.74 mM. Based on these results, in this study, the 200-ns REMD simulation have performed on the isolated Aβ system in a smaller box to save the computing resources.

The effect of $SWCNT_{216}(OH)_{30}$ on $A\beta_{16-22}$ aggregation is also illustrated by the probability of the β-sheet sizes (Fig. 1 *b*). For the isolated Aβ octamer, we find that the two-, three-, and four-stranded β-sheets have probabilities of 21.1%, 13.8%, and 12.0%, respectively. However, in the Aβ+$SWCNT_{216}(OH)_{30}$ complex, the populations of these β-sheets are greatly reduced, to 14.5%, 2.4%, and 0.2%, respectively. Differences are more pronounced for larger sizes of β-sheets. The probabilities of five-, six-, seven-, and eight-stranded β-sheets almost vanish in the Aβ+$SWCNT_{216}(OH)_{30}$ system. These data indicate that $SWCNT_{216}(OH)_{30}$ reduces the populations of all sizes of β-sheets in $A\beta_{16-22}$ octamers.

To probe the influence of $SWCNT_{216}(OH)_{30}$ on the three-dimensional structures of $A\beta_{16-22}$ octamers, we performed cluster analysis on Aβ in the two different systems. Using a C_α root mean-square deviation cutoff of 0.3 nm, we find that the $A\beta_{16-22}$ octamer in the presence of $SWCNT_{216}(OH)_{30}$ can be described by 95 clusters, whereas the isolated $A\beta_{16-22}$ octamer displays 205 clusters. The centers of the first six most populated clusters and their populations are shown in Fig. 1 *c*. These clusters represent 33.8% and 34.1% of all conformations of $A\beta_{16-22}$ octamers in Aβ (Fig. 1 *c*, *upper*) and Aβ+$SWCNT_{216}(OH)_{30}$ systems (Fig. 1 *c*, *lower*), respectively. Without SWCNT*ol*, the Aβ clusters display various ordered and disordered β-sheet-rich conformations. As shown in Fig. 1 *c* (*upper*), the first (C1) and sixth (C6) clusters contain eight- and seven-stranded (configuration type (CT) = 8, 7 + 1) closed/open β-barrels with mixed parallel and antiparallel β-strand alignment, and they have populations of 9.0% and 3.9%, respectively. Clusters C3 and C5 mainly contain bilayer β-sheets (CT = 4 + 3 + 1 and 4 + 4), with populations of 5.2% and 4.1%, respectively. C2 and C4 consist of disordered β-sheet aggregates (CT = 3 + 2(2) + 1, i.e., 3 + 2 + 2 + 1), with probabilities of 7.1% and 4.5%, respectively. In the presence of $SWCNT_{216}(OH)_{30}$ (Fig. 1 *c*, *lower*), $A\beta_{16-22}$ octamers are mostly in amorphous states, consisting of only random chains (C4′) or random chains mixed with two- and three-stranded β-sheets (C1′–C3′, C5′, and C6′), whereas ordered structures including bilayer β-sheets and β-barrels are not observed. Fig. S3 shows that the CLs in the isolated Aβ system mainly vary from 2.828 (CT = 8) to 6.242 (CT = 3 + 2 + 1(3)), indicative of more structured β-sheet-rich conformations, whereas the CLs in the Aβ+$SWCNT_{216}(OH)_{30}$ system are mostly in the range 6.732 (CT = 3 + 1(5)) to 8 (CT = 1(8)), revealing more disordered coil conformations. These results demonstrate that $SWCNT_{216}(OH)_{30}$ distinctly prevents β-sheet formation and shifts the conformations of $A\beta_{16-22}$ octamers from β-sheet-rich to coil-rich aggregates.

To investigate the impact of SWCNT*ol* on the conformational distribution of $A\beta_{16-22}$ octamers, we plot the free-energy landscape as a function of the number of interpeptide hydrogen bonds (H-bonds) and the radius of gyration (Rg) of the $A\beta_{16-22}$ octamers (Fig. 2). The free-energy surfaces of $A\beta_{16-22}$ octamers in the two systems display a quite different shape, narrow in the isolated system but broad in the complex. Although both systems have one deep minimum-energy basin, the locations of these basins are quite different. The minimum-energy basin for the isolated Aβ system is located at (28, 1.0 nm (number of H-bonds, Rg)) (Fig. 2 *a*), whereas that for the Aβ+ SWCNT*ol* complex is located at (10, 1.4 nm) (Fig. 2 *b*). Compared with the $A\beta_{16-22}$ octamer in the absence of SWCNT*ol*, $A\beta_{16-22}$ in the complex has a distinctly decreased number of H-bonds but an increased value of Rg. These results demonstrate that $SWCNT_{216}(OH)_{30}$ disrupts the formation of hydrogen bonds and significantly changes the free-energy landscape of $A\beta_{16-22}$ octamers.

Hydrogen bonding and hydrophobic/aromatic-stacking interactions between the hydroxylated SWCNT and $A\beta_{16-22}$ peptides disrupt the peptide-peptide interactions crucial for β-sheet formation

To explore the primary peptide-peptide interactions destroyed by SWCNT*ol* and the key residues for β-sheet formation, we plot in Fig. 3 the interpeptide main-chain-main-chain (MC-MC) and side-chain-side-chain (SC-SC)

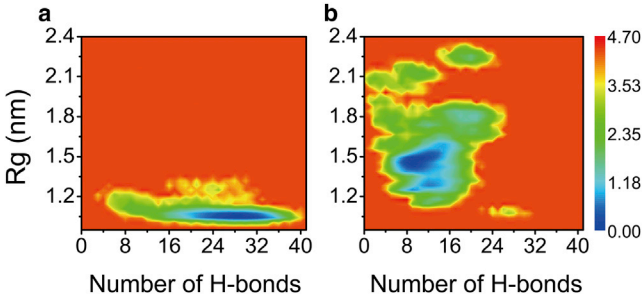

FIGURE 2 Free-energy landscape (kcal/mol) for isolated Aβ octamers (*a*) and Aβ octamers in Aβ+$SWCNT_{216}(OH)_{30}$ complex at 310 K, plotted as a function of the number of interpeptide H-bonds and Rg of the $A\beta_{16-22}$ octamers. To see this figure in color, go online.

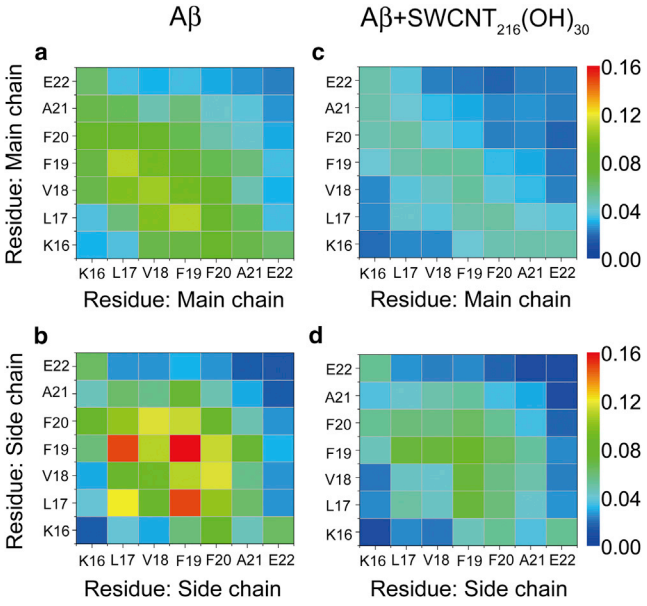

FIGURE 3 MC-MC and SC-SC contact probability maps averaged over 170 ns (30–200 ns) of REMD-generated conformations of Aβ_{16-22} octamer in isolated Aβ (*a* and *b*) and Aβ+SWCNT$_{216}$(OH)$_{30}$ complex (*c* and *d*) at 310 K. To see this figure in color, go online.

contact probabilities between all pairs of residues for Aβ_{16-22} octamers in the absence and presence of SWCNT*ol*. The residue-residue contact probability maps in these two systems display distinct MC-MC and SC-SC interaction patterns, suggesting that SWCNT$_{216}$(OH)$_{30}$ has a strong impact on the interpeptide interactions. Fig. 3, *a* and *b*, shows that Aβ_{16-22} octamers in the absence of SWCNT$_{216}$(OH)$_{30}$ are essentially stabilized by MC-MC interactions of F19-L17 (with a contact probability of 11.0%) and V18-V18 (10.4%) pairs and by SC-SC interactions of F19-F19 (15.9%), L17-F19 (14.8%), and L17-L17 (12.1%) pairs. The relatively high MC-MC contact probabilities along the left diagonal of the contact map in Fig. 3 *a* indicate that Aβ_{16-22} peptides are aligned predominantly in antiparallel orientation. This is consistent with results from a previous experiment showing that the in-register antiparallel pattern is the predominant alignment of β-strands for Aβ_{16-22} peptides at pH ~7.0 (30). It can be seen from Fig. 3 *b* that the F19-F19 pair has the highest SC-SC contact probabilities, reflecting its important role in the aggregation of Aβ_{16-22} peptides, consistent with previous computational and experimental studies (32,44,45). In the presence of SWCNT$_{216}$(OH)$_{30}$, we find that although the peptides still adopt mainly antiparallel alignment, the MC-MC contact probabilities are dramatically reduced (from 11.0% to 5.0% for F19-L17 and from 10.4% to 4.4% for V18-V18) (Fig. 3 *c*). Significantly reduced SC-SC contact probabilities are also observed, with a contact probability of 8.7% (with SWCNT*ol*) versus 15.9% (without SWCNT*ol*) for F19-F19, 7.1% versus 14.8% for F19-L17, and 5.0% versus 12.1% for L17-L17. The dramatic decrease of contact probabilities for these hydrophobic/aromatic residue pairs reflects the influence of hydrophobic interactions between SWCNT*ol* and the hydrophobic/aromatic residues of Aβ_{16-22} peptides. Overall, the presence of SWCNT$_{216}$(OH)$_{30}$ significantly weakens the interpeptide MC-MC and SC-SC interactions, especially the interactions that are critical for β-sheet formation.

After examining the perturbation of SWCNT*ol* on the residue-based peptide-peptide interactions, we further investigate the Aβ-Aβ and Aβ-SWCNT*ol* interactions in terms of number of H-bonds and interaction energy. To this aim, we first calculate the PDF of the number of H-bonds between Aβ-Aβ and Aβ-SWCNT*ol* in isolated Aβ and in the Aβ+SWCNT$_{216}$(OH)$_{30}$ complex. The results are given in Fig. 4, where we can see that in the presence of SWCNT$_{216}$(OH)$_{30}$, the number of interpeptide backbone H-bonds is dramatically reduced to 12 from 28 (without SWCNT*ol*). The decrease in the number of Aβ-Aβ H-bonds is attributed to the formation of H-bonds between the hydroxyl groups of SWCNT$_{216}$(OH)$_{30}$ and the backbone of Aβ_{16-22} peptides (Fig. 4 *a*, *red curve*). We then calculate the interaction energies of Aβ-Aβ and Aβ-SWCNT*ol* and determine the probability distributions (Fig. 4 *b*). The Aβ-Aβ interaction is significantly weakened in the presence of SWCNT$_{216}$(OH)$_{30}$ (Fig. 4 *b*, *black curve with solid squares*) with respect to the isolated Aβ_{16-22} system (Fig. 4 *b*, *black curve with open squares*), due to the competition of the Aβ-SWCNT*ol* interaction (Fig. 4 *b*, *red curve with solid circles*).

To further identify the key residues interacting with SWCNT, we provide the interaction energy between the different amino acid residues and SWCNT$_{216}$(OH)$_{30}$ (Table 1). The interaction energy is decomposed into van der Waals (vdW) and electrostatic interactions. Among all residues, the positively charged residue K16 and the hydrophobic and aromatic residues F19 and F20 have the lowest interaction energies (−8.46, −7.38, and −7.50 kcal/mol), indicating that these three residues have stronger interactions

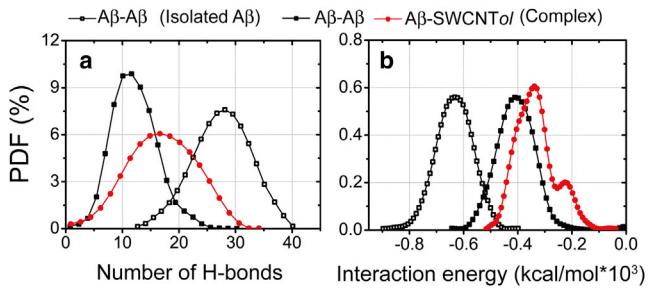

FIGURE 4 PDFs of the number of H-bonds and the interaction energy between Aβ-Aβ and Aβ-SWCNT*ol* in isolated Aβ and Aβ+SWCNT$_{216}$(OH)$_{30}$ complex at 310 K. The number of H-bonds and the interaction energy are averaged over all conformations generated in the last 170 ns (30–200 ns) of the simulation for Aβ octamers in the two different systems. To see this figure in color, go online.

TABLE 1 Interaction energy of each amino acid residue with the hydroxylated SWCNT

	ΔE_{vdW}	ΔE_{elec}	ΔE_{total}
K16	−3.10 (0.31)	−5.36 (0.60)	−8.46 (0.91)
L17	−3.20 (0.25)	−1.50 (0.09)	−4.70 (0.34)
V18	−2.95 (0.28)	−2.36 (0.19)	−5.31 (0.47)
F19	−5.03 (0.51)	−2.35 (0.21)	−7.38 (0.72)
F20	−4.55 (0.40)	−2.95 (0.27)	−7.50 (0.67)
A21	−1.97 (0.13)	−1.80 (0.11)	−3.77 (0.24)
E22	−3.17 (0.41)	−2.03 (0.15)	−5.20 (0.56)

Interaction energy includes van der Waals (ΔE_{vdW}), electrostatic (ΔE_{elec}), and total (ΔE_{total}) energy in kcal/mol. Numbers in parentheses indicate the standard error.

with $SWCNT_{216}(OH)_{30}$ compared to the other residues. Among these three residues, K16 has the lowest electrostatic interaction energy (−5.36 kcal/mol) and residues F19 and F20 have the lowest vdW interaction energies (−5.03 and −4.55 kcal/mol). These results indicate that the interactions of A$\beta_{16–22}$ peptides with the hydroxylated SWCNT are mostly driven by electrostatic interactions between K16 and SWCNT*ol*, in addition to the hydrophobic and aromatic stacking interactions between F19 and F20 and SWCNT*ol*, although other residues also participate in the Aβ-SWCNT*ol* interactions. It has been demonstrated that interpeptide hydrogen-bonding and hydrophobic and aromatic stacking interactions play important roles in the formation and stabilization of A$\beta_{16–22}$ fibrils (32,46–50). The strong Aβ-SWCNT*ol* interactions shown in Fig. 4 and Table 1 would hinder the interpeptide interactions responsible for A$\beta_{16–22}$ aggregation, therefore slowing down the nucleation and fibrillization process.

AFM and ThT fluorescence experiments demonstrate that hydroxylated SWCNTs can efficiently inhibit the fibrillization of A$\beta_{16–22}$ peptides

Our REMD simulation results show that SWCNT*ol* ($SWCNT_{216}(OH)_{30}$) significantly shift the conformations of early formed A$\beta_{16–22}$ oligomers from ordered β-sheet-rich structures to disordered coil aggregates. AFM imaging and ThT fluorescence measurements are employed to confirm the simulation results. Fig. 5 shows AFM images of A$\beta_{16–22}$ samples incubated with and without hydroxylated SWCNTs for three different incubation time periods (*upper three rows*) and section analyses of A$\beta_{16–22}$ aggregates at 10 h (*lower*). The mass fractions of SWCNTs and the hydroxyl groups in the hydroxylated SWCNTs are 86.04 wt % and 3.96 wt %, respectively. For the sake of comparison with simulation results, we convert the mass fraction to the ratio of the number of carbon atoms to the number of hydroxyl groups (OH). The converted expression is $SWCNT_{216}(OH)_7$. As seen in Fig. 5 (*upper rows*), for A$\beta_{16–22}$ samples without SWCNTs, both small and large

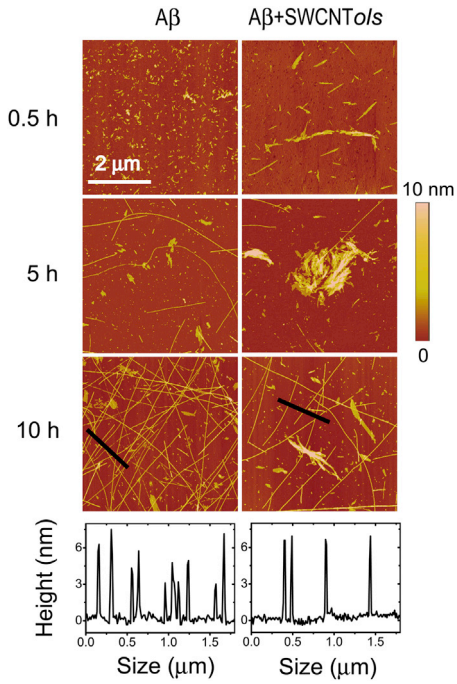

FIGURE 5 AFM images of A$\beta_{16–22}$ aggregate with/without $SWCNT_{216}(OH)_7$ at three different coincubation time points (0.5 h, 5 h, and 10 h). Section analyses of A$\beta_{16–22}$ aggregates at 10 h are given on the bottom. To see this figure in color, go online.

aggregates are observed at $t = 0.5$ h. With increasing incubation time, short and long fibrils appear at $t = 5$ h and a significant number of long and thin fibrils are observed at $t =$ 10 h. Conversely, in the presence of $SWCNT_{216}(OH)_7$, only short fibrils and small aggregates with various sizes are observed within the initial 5 h. As the incubation time increases to 10 h, long fibrils appear but their number is much smaller than in the absence of $SWCNT_{216}(OH)_7$. The profiles along the marked lines in the AFM images at 10 h incubation are given in the bottom row of Fig. 5, and it can be seen that within the same length of 2 μm, nine fibrils are observed in the absence of $SWCNT_{216}(OH)_7$, whereas only four fibrils are observed in the presence of $SWCNT_{216}(OH)_7$, indicating that hydroxylated SWCNTs can significantly suppress the formation of mature fibrils.

For comparison, we also give the corresponding AFM images of A$\beta_{16–22}$ samples in the presence of pristine SWCNT (Fig. S4). With respect to the end product of A$\beta_{16–22}$ samples without SWCNTs, the number of long fibrils is also greatly reduced, indicating that pristine SWCNTs can prevent the fibrillization of A$\beta_{16–22}$ peptides, in support of our previous REMD simulation results (21). Compared with A$\beta_{16–22}$ samples with pristine SWCNTs, the number of long fibrils at $t = 10$ h in the presence of $SWCNT_{216}(OH)_7$ is decreased, implying that hydroxylated SWCNTs can more effectively inhibit the formation of mature fibrils. It should be noted that apart from the protofibrils or long fibrils, a large number of platelike aggregates

are also observed during the coincubation process ($t = 0.5$, 5, and 10 h) with pristine SWCNTs. We conjecture that these platelike aggregates mainly consist of SWCNT self-aggregates due to the low solubility of pristine (or bare) SWCNTs. Hence, it is necessary to modify the surface of pristine SWCNT to enhance its solubility. Overall, our AFM results in Figs. 5 and S4 demonstrate that both pristine and hydroxylated SWCNTs can significantly inhibit the fibrillization of $A\beta_{16-22}$ peptides, confirming our previous (21) and present simulation results.

The inhibitory effect of hydroxylated SWCNTs on the aggregation of $A\beta_{16-22}$ peptides is further examined by monitoring ThT fluorescence intensity in solution. Fig. 6 shows the ThT fluorescence spectra of $A\beta_{16-22}$ samples with/without $SWCNT_{216}(OH)_7$ at incubation times of 5 h and 10 h. For comparison, the background fluorescence spectrum of ThT is also given. It can be seen from Fig. 6 *a* that at $t = 5$ h, the addition of $SWCNT_{216}(OH)_7$ in $A\beta_{16-22}$ solution results in a significant suppression of fluorescence intensity, indicating that the formation of β-sheet structures is dramatically retarded by $SWCNT_{216}(OH)_7$. When the coincubation time increases further, to 10 h, the fluorescence intensities in both systems increase, which is consistent with the formation of mature fibrils seen in the AFM images in Fig. 5. However, the intensity increment in the $A\beta$+$SWCNT_{216}(OH)_7$ system is far smaller than that in the $A\beta$ system (Fig. 6 *b*), implying that hydroxylated SWCNTs significantly retard the fibril formation of $A\beta_{16-22}$ peptides. In addition, we present in Fig. S5 the emission spectra of ThT bound to $A\beta_{16-22}$ in the presence of pristine SWCNTs at 5 h and 10 h. One can see that the fluorescence intensity in the $A\beta$+SWCNT system is greater than that in the $A\beta$+$SWCNT_{216}(OH)_7$ system, indicating that hydroxylated SWCNT has a stronger inhibitory effect on the β-sheet formation of $A\beta_{16-22}$ compared to pristine SWCNT.

Our previous REMD study showed that pristine SWCNTs inhibited the formation of β-sheet-rich $A\beta_{16-22}$ oligomers. The obtained average β-sheet content was 7.9% (21), smaller than the value of 17.8% observed in the presence of hydroxylated SWCNTs. The difference between this finding and the AFM and ThT results may be attributed to the following factors. The stronger β-sheet inhibition of pristine SWCNTs (7.9% of β-sheet content) relative to hydroxylated SWCNTs (17.8% of β-sheet content) predicted from simulations is for a single and short SWCNT, whereas in the AFM experiments, multiple pristine SWCNTS were used. These pristine SWCNTs can self-aggregate readily into aggregates (see the platelike aggregates in Fig. S4; more details about the aggregates remain to be determined) in aqueous solution due to their low solubility, whereas the hydroxylated SWCNTs are more water-soluble and can be better dispersed in aqueous solution. The formation of aggregates would result in a reduced total surface area of pristine SWCNTs with respect to the dispersed hydroxylated SWCNTs. The significantly decreased surface area of pristine SWCNTs would weaken SWCNT-$A\beta_{16-22}$ interactions critical for β-sheet inhibition, thus reducing the inhibitory effect of pristine SWCNTs. Despite this inconsistency, both our simulation and the experimental data consistently demonstrate that hydroxylated SWCNTs can dramatically inhibit β-sheet formation of $A\beta_{16-22}$ peptides. We also note that the extent of hydroxylation of SWCNTs used in REMD simulations is different from that in AFM experiments. For a direct comparison of the simulation and experimental results, we performed a preliminary 70-ns REMD simulation on $A\beta_{16-22}$ octamer with $SWCNT_{216}(OH)_7$. Based on the last 40 ns of the trajectory, we calculated the average β-sheet probability as 13.5%, much lower than the β-sheet content of 46.6% found for $A\beta_{16-22}$ octamer without carbon nanotubes. This preliminary REMD simulation demonstrates that $SWCNT_{216}(OH)_7$ can also dramatically retard the aggregation of $A\beta_{16-22}$ peptides. Taken together, our REMD simulations and AFM experiments demonstrate that both pristine and hydroxylated SWCNTs can inhibit the aggregation of $A\beta_{16-22}$ peptides. It has been reported that $A\beta_{16-22}$ is the central hydrophobic core of the full-length Aβ40/42 (30,51). The β-strands in $A\beta_{16-22}$ fibrils formed at neutral pH are in antiparallel alignment (30), whereas the full-length $A\beta$ fibrils have a β-strand-turn-β-strand motif, with β-strands in parallel alignment (52). Thus, whether carbon nanoparticles can reduce the β-sheet formation of full-length $A\beta$ and inhibit its fibrillization remains to be determined.

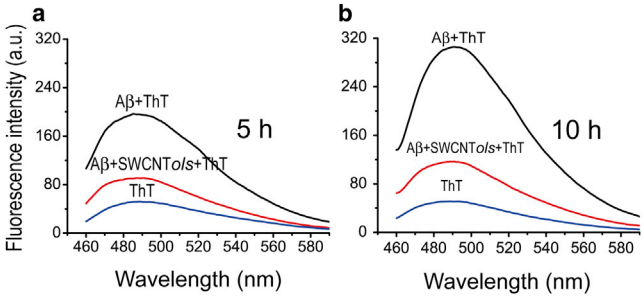

FIGURE 6 Emission spectra of ThT in $A\beta_{16-22}$ solution with and without $SWCNT_{216}(OH)_7$ at incubation times of 5 h (*a*) and 10 h (*b*). The background fluorescence of ThT is also shown. To see this figure in color, go online.

CONCLUSIONS

To conclude, we have studied the effects of hydroxylated SWCNT (a water-soluble SWCNT derivative) on the aggregation of $A\beta_{16-22}$ peptides. Extensive REMD simulations on the oligomerization of $A\beta_{16-22}$ peptides in the absence and presence of SWCNTs demonstrate that hydroxylated SWCNTs have strong H-bonding interaction with the backbone of $A\beta_{16-22}$ and hydrophobic/aromatic stacking interaction with the side chains of F19 and F20 residues. The hydroxyl groups of SWCNTs also display strong

electrostatic interactions with the positively charged residue K16. As interpeptide MC-MC and SC-SC interactions determine the aggregation properties, i.e., the populations of ordered β-sheet-rich and disordered coil oligomers and the rate of fibrillization, the strong SWCNT*ol*-A$\beta_{16–22}$ interactions would interfere with the interpeptide interactions that are crucial for A$\beta_{16–22}$ aggregation, thus retarding the nucleation and fibrillization process. Our AFM and ThT fluorescence experiments provide direct evidence of the strong inhibitory effect of hydroxylated SWCNTs on the aggregation of A$\beta_{16–22}$ peptides. Taken as a whole, our study demonstrates that both pristine and hydroxylated SWCNTs can prevent the aggregation of A$\beta_{16–22}$ peptides. This study also provides molecular insights into the inhibition mechanism of hydroxylated SWCNTs on A$\beta_{16–22}$ fibrillization and will be helpful in designing therapeutic agents to treat AD.

SUPPORTING MATERIAL

Five figures and Supporting Methods are available at http://www.biophysj.org/biophysj/supplemental/S0006-3495(14)00939-4.

Simulations were performed at the National High Performance Computing Center of Fudan University.

This work was supported by the National Science Foundation of China (grants 91227102 and 11274075).

SUPPORTING CITATIONS

References (53–56) appear in the Supporting Material.

REFERENCES

1. Chiti, F., and C. M. Dobson. 2006. Protein misfolding, functional amyloid, and human disease. *Annu. Rev. Biochem.* 75:333–366.
2. Pitschke, M., R. Prior, …, D. Riesner. 1998. Detection of single amyloid β-protein aggregates in the cerebrospinal fluid of Alzheimer's patients by fluorescence correlation spectroscopy. *Nat. Med.* 4:832–834.
3. Lührs, T., C. Ritter, …, R. Riek. 2005. 3D structure of Alzheimer's amyloid-β(1-42) fibrils. *Proc. Natl. Acad. Sci. USA.* 102:17342–17347.
4. Grant, M. A., N. D. Lazo, …, D. B. Teplow. 2007. Familial Alzheimer's disease mutations alter the stability of the amyloid β-protein monomer folding nucleus. *Proc. Natl. Acad. Sci. USA.* 104:16522–16527.
5. Cabaleiro-Lago, C., F. Quinlan-Pluck, …, S. Linse. 2008. Inhibition of amyloid β protein fibrillation by polymeric nanoparticles. *J. Am. Chem. Soc.* 130:15437–15443.
6. Kim, J. E., and M. Lee. 2003. Fullerene inhibits β-amyloid peptide aggregation. *Biochem. Biophys. Res. Commun.* 303:576–579.
7. Ghule, A. V., K. M. Kathir, …, Y.-C. Ling. 2007. Carbon nanotubes prevent 2, 2, 2 trifluoroethanol induced aggregation of protein. *Carbon.* 45:1586–1589.
8. Linse, S., C. Cabaleiro-Lago, …, K. A. Dawson. 2007. Nucleation of protein fibrillation by nanoparticles. *Proc. Natl. Acad. Sci. USA.* 104:8691–8696.
9. Liao, Y. H., Y. J. Chang, …, Y. R. Chen. 2012. Negatively charged gold nanoparticles inhibit Alzheimer's amyloid-β fibrillization, induce fibril dissociation, and mitigate neurotoxicity. *Small.* 8:3631–3639.
10. Ma, Q., G. Wei, and X. Yang. 2013. Influence of Au nanoparticles on the aggregation of amyloid-β-(25–35) peptides. *Nanoscale.* 5:10397–10403.
11. Cabaleiro-Lago, C., O. Szczepankiewicz, and S. Linse. 2012. The effect of nanoparticles on amyloid aggregation depends on the protein stability and intrinsic aggregation rate. *Langmuir.* 28:1852–1857.
12. Liu, R., R. Su, …, Z. He. 2012. Physicochemical strategies for inhibition of amyloid fibril formation: an overview of recent advances. *Curr. Med. Chem.* 19:4157–4174.
13. Li, C., and R. Mezzenga. 2013. The interplay between carbon nanomaterials and amyloid fibrils in bio-nanotechnology. *Nanoscale.* 5:6207–6218.
14. Mahmoudi, M., H. R. Kalhor, …, I. Lynch. 2013. Protein fibrillation and nanoparticle interactions: opportunities and challenges. *Nanoscale.* 5:2570–2588.
15. Zhang, M., X. Mao, …, C. Wang. 2013. Nanomaterials for reducing amyloid cytotoxicity. *Adv. Mater.* 25:3780–3801.
16. Porter, A. E., M. Gass, …, M. Welland. 2007. Direct imaging of single-walled carbon nanotubes in cells. *Nat. Nanotechnol.* 2:713–717.
17. Kam, N. W. S., and H. Dai. 2005. Carbon nanotubes as intracellular protein transporters: generality and biological functionality. *J. Am. Chem. Soc.* 127:6021–6026.
18. Harrison, B. S., and A. Atala. 2007. Carbon nanotube applications for tissue engineering. *Biomaterials.* 28:344–353.
19. Pagona, G., and N. Tagmatarchis. 2006. Carbon nanotubes: materials for medicinal chemistry and biotechnological applications. *Curr. Med. Chem.* 13:1789–1798.
20. Fu, Z., Y. Luo, …, G. Wei. 2009. Induced β-barrel formation of the Alzheimer's A$\beta_{25–35}$ oligomers on carbon nanotube surfaces: implication for amyloid fibril inhibition. *Biophys. J.* 97:1795–1803.
21. Li, H., Y. Luo, …, G. Wei. 2011. Carbon nanotube inhibits the formation of β-sheet-rich oligomers of the Alzheimer's amyloid-$\beta_{16–22}$ peptide. *Biophys. J.* 101:2267–2276.
22. Andujar, S. A., F. Lugli, …, F. Zerbetto. 2012. Amyloid-β fibril disruption by C_{60}-molecular guidance for rational drug design. *Phys. Chem. Chem. Phys.* 14:8599–8607.
23. Guo, J., J. Li, …, X. Yao. 2013. Exploring the influence of carbon nanoparticles on the formation of β-sheet-rich oligomers of IAPP$_{22–28}$ peptide by molecular dynamics simulation. *PLoS ONE.* 8:e65579.
24. Jana, A. K., and N. Sengupta. 2012. Adsorption mechanism and collapse propensities of the full-length, monomeric A$\beta_{1–42}$ on the surface of a single-walled carbon nanotube: a molecular dynamics simulation study. *Biophys. J.* 102:1889–1896.
25. Jana, A. K., J. C. Jose, and N. Sengupta. 2013. Critical roles of key domains in complete adsorption of Aβ peptide on single-walled carbon nanotubes: insights with point mutations and MD simulations. *Phys. Chem. Chem. Phys.* 15:837–844.
26. Jana, A. K., and N. Sengupta. 2013. Surface induced collapse of A$\beta_{1–42}$ with the F19A replacement following adsorption on a single walled carbon nanotube. *Biophys. Chem.* 184:108–115.
27. Todorova, N., A. J. Makarucha, …, I. Yarovsky. 2013. Dimensionality of carbon nanomaterials determines the binding and dynamics of amyloidogenic peptides: multiscale theoretical simulations. *PLOS Comput. Biol.* 9:e1003360.
28. Zuo, G., X. Zhou, …, R. Zhou. 2011. Adsorption of villin headpiece onto graphene, carbon nanotube, and C_{60}: effect of contacting surface curvatures on binding affinity. *J. Phys. Chem. C.* 115:23323–23328.
29. Liu, Z., Y. Liu, and D. Peng. 2014. Hydroxylation of multi-walled carbon nanotubes reduces their cytotoxicity by limiting the activation of mitochondrial mediated apoptotic pathway. *J. Mater. Sci. Mater. Med.* 25:1033–1044.
30. Balbach, J. J., Y. Ishii, …, R. Tycko. 2000. Amyloid fibril formation by A$\beta_{16–22}$, a seven-residue fragment of the Alzheimer's β-amyloid peptide, and structural characterization by solid state NMR. *Biochemistry.* 39:13748–13759.
31. Röhrig, U. F., A. Laio, …, R. Petronzio. 2006. Stability and structure of oligomers of the Alzheimer peptide Aβ_{16-22}: from the dimer to the 32-mer. *Biophys. J.* 91:3217–3229.

32. Xie, L., Y. Luo, and G. Wei. 2013. $A\beta_{16-22}$ peptides can assemble into ordered β-barrels and bilayer β-sheets, while substitution of phenylalanine 19 by tryptophan increases the population of disordered aggregates. *J. Phys. Chem. B.* 117:10149–10160.

33. Berendsen, H., J. Postma, …, J. Hermans. 1981. Interaction models for water in relation to protein hydration. *Intermol. Forces.* 11:331–342.

34. Sugita, Y., and Y. Okamoto. 1999. Replica-exchange molecular dynamics method for protein folding. *Chem. Phys. Lett.* 314:141–151.

35. Lindahl, E., B. Hess, and D. Van Der Spoel. 2001. GROMACS 3.0: a package for molecular simulation and trajectory analysis. *J. Mol. Model.* 7:306–317.

36. van Gunsteren, W. F., S. R. Billeter, …, I. G. Tironi. 1996. Biomolecular Simulation: The {GROMOS96} Manual and User Guide. Verlag der Fachvereine Hochschulverlag, AG an der ETH Zürich, Zürich, Switzerland.

37. Nguyen, P. H., M. S. Li, …, D. Thirumalai. 2007. Monomer adds to preformed structured oligomers of Aβ-peptides by a two-stage dock-lock mechanism. *Proc. Natl. Acad. Sci. USA.* 104:111–116.

38. Krone, M. G., L. Hua, …, J.-E. Shea. 2008. Role of water in mediating the assembly of Alzheimer amyloid-β $A\beta_{16-22}$ protofilaments. *J. Am. Chem. Soc.* 130:11066–11072.

39. Qiao, R., A. P. Roberts, …, P. C. Ke. 2007. Translocation of C_{60} and its derivatives across a lipid bilayer. *Nano Lett.* 7:614–619.

40. Kabsch, W., and C. Sander. 1983. Dictionary of protein secondary structure: pattern recognition of hydrogen-bonded and geometrical features. *Biopolymers.* 22:2577–2637.

41. Lu, Y., P. Derreumaux, …, G. Wei. 2008. Thermodynamics and dynamics of amyloid peptide oligomerization are sequence dependent. *Proteins.* 75:954–963.

42. Humphrey, W., A. Dalke, and K. Schulten. 1996. VMD: visual molecular dynamics. *J. Mol. Graph.* 14:33–38, 27–28.

43. Matthes, D., V. Gapsys, and B. L. de Groot. 2012. Driving forces and structural determinants of steric zipper peptide oligomer formation elucidated by atomistic simulations. *J. Mol. Biol.* 421:390–416.

44. Williams, A. D., E. Portelius, …, R. Wetzel. 2004. Mapping Aβ amyloid fibril secondary structure using scanning proline mutagenesis. *J. Mol. Biol.* 335:833–842.

45. Inouye, H., K. A. Gleason, …, D. A. Kirschner. 2010. Differential effects of Phe19 and Phe20 on fibril formation by amyloidogenic peptide $A\beta_{16-22}$ (Ac-KLVFFAE-NH_2). *Proteins.* 78:2306–2321.

46. Favrin, G., A. Irbäck, and S. Mohanty. 2004. Oligomerization of amyloid $A\beta_{16-22}$ peptides using hydrogen bonds and hydrophobicity forces. *Biophys. J.* 87:3657–3664.

47. Gnanakaran, S., R. Nussinov, and A. E. García. 2006. Atomic-level description of amyloid β-dimer formation. *J. Am. Chem. Soc.* 128:2158–2159.

48. Chaudhary, N., and R. Nagaraj. 2011. Impact on the replacement of Phe by Trp in a short fragment of Aβ amyloid peptide on the formation of fibrils. *J. Pept. Sci.* 17:115–123.

49. Senguen, F. T., T. M. Doran, …, B. L. Nilsson. 2011. Clarifying the influence of core amino acid hydrophobicity, secondary structure propensity, and molecular volume on amyloid-β 16–22 self-assembly. *Mol. Biosyst.* 7:497–510.

50. Berhanu, W. M., and U. H. Hansmann. 2012. Side-chain hydrophobicity and the stability of $A\beta_{16-22}$ aggregates. *Protein Sci.* 21:1837–1848.

51. Anthony, N. R., A. K. Mehta, …, K. M. Berland. 2014. Mapping amyloid-β_{16-22} nucleation pathways using fluorescence lifetime imaging microscopy. *Soft Matter.* 10:4162–4172.

52. Tycko, R. 2011. Solid-state NMR studies of amyloid fibril structure. *Annu. Rev. Phys. Chem.* 62:279–299.

53. Miyamoto, S., and P. A. Kollman. 1992. SETTLE: an analytical version of the SHAKE and RATTLE algorithm for rigid water models. *J. Comput. Chem.* 13:952–962.

54. Hess, B., H. Bekker, …, J. G. Fraaije. 1997. LINCS: a linear constraint solver for molecular simulations. *J. Comput. Chem.* 18:1463–1472.

55. Berendsen, H. J., J. P. M. Postma, …, J. Haak. 1984. Molecular dynamics with coupling to an external bath. *J. Chem. Phys.* 81:3684–3690.

56. Daura, X., K. Gademann, …, A. E. Mark. 1999. Peptide folding: when simulation meets experiment. *Angew. Chem. Int.* 38:236–240.